The University of Texas at San Antonio

Three-Dimensional Model of a Faulted Miocene Tuff Layer at Yucca Mountain, Nevada

by

Shannon Lindsay Colton

An Honors Thesis

Submitted to the Faculty of the University Honors Program

in Partial Fulfillment of the Requirements

for

Graduation with University Honors Program Honors

Approved: Stuart Birnbaum May 27, 1998

Signature of Dr. Stuart J. Birnbaum Date

Signature of Dr. David A. Ferrill

Signature of Dr. Eric R. Swanson

Spring 1998

Abstract--A three-dimensional model of five major faults, several smaller faults, and the contact between crystal-rich (Cr) and crystal-poor (Cp) Tiva Canyon Tuff was developed to reveal the geometry of fault blocks and unravel the kinematic development of major fault systems on western Yucca Mountain, Nevada. Geometry of fault blocks and net displacement along fault surfaces indicates that the western Yucca Mountain fault system is in an advanced state of fault development by segment linkage. Linkage has occurred by both curved tip propagation and connecting fault formation and has produced breached relay ramps. A cumulative throw profile reveals two local minima, where there are probably additional fault segments and/or deformation within relay ramps buried beneath Quaternary alluvium.

INTRODUCTION

Yucca Mountain is a faulted east-dipping cuesta in southwest Nevada composed of Miocene ash flow tuff layers. Yucca Mountain is in the western Basin and Range Province, an area with complex Miocene to present extensional and strike-slip faulting (Scott, 1990; Ferrill *et al.*, 1996; Morris *et al.*, 1996). The ridge capping layers at Yucca Mountain consist of various thermomechanical units of the Miocene Tiva Canyon Tuff (Day *et al.*, 1998). The faults at Yucca Mountain have been carefully mapped, however the relationships between major throughgoing faults and smaller faults or fault branches remains poorly constrained. Three-dimensional (3D) models of fault blocks in Yucca Mountain have been of relatively low resolution, limited by the number of faults included and data density on faulted horizons (Stirewalt *et al.*, 1994). The gross structural history of Yucca Mountain is fairly well known (Ferrill *et al.*, 1997; Stirewalt *et al.*,

1994; Scott, 1990), but the detailed evolution of the Yucca Mountain fault system remains relatively unstudied.

For this study, a detailed 3D model of a single faulted horizon in the Tiva Canyon Tuff cut by five major faults was created to analyze current fault relationships and the kinematic development of the fault system in western Yucca Mountain. Fault plane dips were analyzed, and cumulative throw profiles and geometry of fault blocks derived from the 3D model are discussed in terms of stages of fault development on western Yucca Mountain.

FAULT DIP ANALYSIS

An analysis of fault orientation was conducted to identify any consistent patterns of dip change north or south along western Yucca Mountain faults. Fault strike and dip data for Yucca Mountain faults were available from two maps (Simonds *et al.*, 1995; Day *et al.*, 1998). The digital version of the 1:24,000 scale map of Yucca Mountain faults by Simonds *et al.* (1995) was in Universal Transverse Mercator (UTM), North American Datum of 1983 (NAD83). The 1:24,000 scale geologic map of Yucca Mountain by Day *et al.* (1998) was projected in State Plane coordinates, NAD83, and was converted to UTM, NAD83 to provide a common coordinate system for data analysis. Strikes and dips of fault planes and coordinates of mapped fault traces were collected for the Northern Windy Wash, Fatigue Wash, Boomerang Point, Solitario Canyon, and Iron Ridge faults between UTM coordinates 544757 to 547452 and 4071368 to 4083696 (Table 1). Fault dip was plotted versus latitude for each of these faults (Fig. 1). Limited data were available for the Fatigue Wash fault (three measurements) and Boomerang Point fault (one measurement). Numerous fault orientation measurements were available for

Northern Windy Wash, Solitario Canyon, and Iron Ridge faults. Orientation data for the Northern Windy Wash fault displays an increase in fault dip to the south, but other faults do not show a pronounced increase or decrease to the south. Solitario Canyon and Iron Ridge fault dips vary widely within short distances (e.g. 25° in 200m). Due to the lack of data along some faults and the high variance of dip along other faults, the average dip for each fault was calculated, and each fault in the 3D model is portrayed with its average dip value along the entire length of the fault.

THREE-DIMENSIONSL MODEL DEVELOPMENT

A 3D model was developed to study the geometry of faults and fault blocks along western Yucca Mountan. The five major faults in the study area are the Northern Windy Wash, Fatigue Wash, Boomerang Point, Solitario Canyon, and Iron Ridge faults. The bottom of the Cr unit, a crystal-rich member of the Tiva Canyon Tuff, was the horizon selected from a 1:24,000 scale map of Yucca Mountain as the horizon with maximum outcrop exposure data to constrain the 3D horizon model (Day *et al.*, 1998). The map was available in digital format as a "dxf" file, indicating its origin as an AutoCad file. With ArcInfo version 7.0.2 software, the "dxf" file was converted to coverages containing the coordinates of fault dips, faults, and structural contour lines, all projected in State Plane coordinates, NAD83.

ArcEdit version 7.0.2 was used to delete from coverages all structural contour arcs except the bottom of Cr, and all faults except the five major faults listed above. The data would ultimately be modeled with EarthVision version 4.0.3 software, in which acceptable input

includes lines with a constant elevation and points. Points along each Cr-Cp contact varied in elevation. Thus, individual data points with unique elevations were necessary for the EarthVision model. Arcs were converted to sets of data points sampled along each arc. Elevations for each data point along arcs were sampled from a digital elevation map (DEM) of Yucca Mountain, with map coordinates and elevations sampled on a 30 meter grid. The DEM was projected in UTM zone 11, NAD83. The structural contour, fault, and fault dip maps were converted to UTM zone 11, NAD83 with the "NADCON" command in ArcInfo. Then, the "LATTICESPOT" command in ArcInfo was used to calculate each point elevation by reference to the DEM. A nawk code (written by Ronald Martin, CNWRA) was used to convert the file to a format suitable for EarthVision.

In EarthVision, several specific data points and the overall morphology of the horizon were checked by visual comparison to the 1:24,000 scale map. Individual faults were stored in separate data files. Two-dimensional (2D) grids were drawn for each fault. The grids accurately fit the data points for the fault; however control points were necessary to constrain the fault location at depth and height above the surface. To constrain 3D fault geometry, a nawk code was written to extrapolate each fault data point both up and down the fault surface based on the strike and dip of each fault. For each fault, this was performed to heights of 200m and 1000m, and to a depth of 1000m from the original data. The data at these three locations were concatenated to the original data, and the points were connected by 2D gridding. Since 2D grids cover the entire range of the model, EarthVision's Graphic Editor was used to draw clipping polygons which specified the range of faults to be used in further calculations, such as horizon gridding. For example, the Boomerang Point fault is contained in approximately the middle third

(from north to south) of the model. Some faults extend beyond the range of the model. For example, the Iron Ridge fault continues south of the model. In this case, a clipping polygon was drawn for the fault to continue north until it no longer appears at the surface, and terminate at some distance south of the model. EarthVision Geologic Structure Builder was used to establish a fault tree hierarchy, in which faulting order was specified. For example, Iron Ridge fault was set to terminate at the intersection of Iron Ridge and Solitario Canyon faults. A 3D model was calculated as specified by the fault tree hierarchy.

The contact between Cr and Cp was then edited and added to the model. Horizon data points along fault surfaces were removed as required in EarthVision to ensure calculation of a reasonable plane. Points along fault surfaces, if not removed, might be used within the wrong block during calculations and the resulting horizon can make steep, unsuitable curves to connect those points. Information about the horizon was added in the Geologic Structure Builder, and a horizon was calculated to fit the data points within the 3D fault structure previously built.

Distinct curves in the horizon surface remained at this point. For example, the data points between Solitario Canyon fault and Iron Ridge fault had several relatively abrupt decreases in elevation, indicative of fault offset. Faults in these locations were also mapped by Day *et al.* (1998) on the 1:24,000 scale geologic map. The largest of these faults was gathered from the converted Arc coverage by Day *et al.* (1998) and converted to EarthVision data points. No dip values were available for this fault. Other faults oriented in the same direction (NW) commonly have dips of 80 degrees. Thus, an 80 degree dip was applied to this fault. Another major flaw in the horizon was due to a complex system of faults between Northern Windy Wash and Fatigue Wash faults. Although there are many faults in that area, no single one was isolated

for the model. Instead, a connecting fault was modeled in the approximate area of the faults, and it was added to the model with a constant dip of 80 degrees. The resulting fault model showed connections between major faults (Fig. 2). The horizon was regridded, and revealed the largest undulations in the horizon surface had been removed by the addition of these faults (Fig. 3). There are several less pronounced steps remaining in the fault surface. For example, there are indications of faults in two areas north of Boomerang Point fault. These correspond in position to clusters of faults north of Boomerang Point fault on the 1:24,000 scale geologic map by Simonds et al. (1995).

FAULT GROWTH BY SEGMENT LINKAGE

During the last decade, there have been major advances in the understanding of the evolution and interaction of normal faults and fault systems (Childs *et al.*, 1997; Peacock and Sanderson, 1994; Trudgill and Cartwright, 1994) and scaling relationships for normal faults (Scholz *et al.*, 1993; Dawers and Anders, 1995; Dawers *et al.*, 1993). There are two end-member conceptual models of fault development. One is a single fault that grows larger as slip increases. The other is fault growth by segment linkage (Willemese *et al.*, 1995). Trudgill and Cartwright (1994) and Peacock and Sanderson (1994) describe the process of segment linkage, based on field work on faults varying from the meter scale to the kilometer scale. First, segments are unconnected and do not interact. The fault segments grow, and when interaction occurs near the tips, the segments are "soft-linked" by an area of complex deformation, such as a relay ramp. A relay ramp is the volume of rock between two overlapping fault segments that show

displacement transfer (Childs *et al.*, 1995). The relay ramp area experiences rotation (tilting) about an axis nearly perpendicular to the fault planes. The rock is often tilted toward the hanging wall and fractured. Both overlapping and underlapping "soft-linked" faults tend to show the steepest displacement gradients off-centered, toward relay structures (Willemese, 1997). As segment displacement continues, relay ramps develop faults. A "hard-linked" fault system exists when one or more connecting faults have developed between the original faults segments, or a fault tip curves until joining the other segment, directly transferring displacement between the two faults. Breakthrough by curved lateral propagation can leave only one relict fault tip in the area of overlap, whereas breakthrough by connecting fault formation can leave two relict fault tips. In both cases, relict relay ramps can remain on the hangingwall or footwall (Fig. 4) (Ferrill *et al.*, 1998).

Examples of segment linkage both by connecting fault formation and curved lateral propagation are present at Yucca Mountain. For example, the Northern Windy Wash and Fatigue Wash faults are joined by a complex system of connecting faults, and Iron Ridge joins Solitario Canyon by curved tip propagation (Ferrill *et al.*, 1998).

The Solitario Canyon fault can be divided into three segments separated by cusps: northern, middle, and southern segments. Where the segments join, the westward triangular protrusions are referred to as a "cusps." We interpret that the Solitario Canyon northern segment and splay formed as a single fault, isolated from the middle segment. The northern tip of middle segment grew to connect with the northern segment and splay. Once the two faults were "hard-linked" and the relay ramp was breached, the splay probably became relatively inactive.

The Iron Ridge fault seems to be in an earlier stage of the same process. Displacement on the southern segment of Solitario Canyon fault might decline or cease as the Iron Ridge accumulates more displacement. Over time, Iron Ridge fault would develop a larger net displacement, while the southern segment of the Solitario Canyon fault would experience decreased faulting activity until only a inactive relict tip may exist. Aside from a relict tip, another noticeable feature is the cusp where the faults intersect.

Northern Windy Wash and Fatigue Wash faults are connected by a complex area of faulting, with an overall trend to the NW (Ferrill *et al.*, 1998). Although these two faults are now connected by a throughgoing connecting fault system, the fault linkage has apparently not led to segment abandonment on Northern Windy Wash fault. Mapping by Simonds *et al.* (1995) suggests that the segments of the Northern Windy Wash fault, both north and south of the connecting fault system, and the Fatigue Wash fault south of the connecting fault system, have been active in the late Quaternary. The northern part of the Fatigue Wash fault is interpreted by Simonds et al.(1995) to display no evidence of Quaternary displacement, consistent with an interpretation that formation of the current fault system has led to abandonment of the northern segment of the Fatigue Wash fault.

THROW VERSUS DISTANCE DIAGRAMS

Throw versus distance diagrams can be used to interpret fault interactions. Generally, faults may be unlinked, or linked by a branch point or a branch line (Childs *et al.*, 1997). Linked faults can be plotted on a throw versus distance diagram to study displacement patterns

for the fault system. For a linked fault system, the curves for each linked fault are added together to form a cumulative profile. The cumulative profile generally resembles the profile expected for one fault; maximum displacement occurs near the center, with zero displacement on the ends. The cumulative fault throw profile for a segmented fault system, however, is more complex than a single fault throw profile (Dawers and Anders, 1995). If deformations within relay ramps are not included in the cumulative profile, there are often, but not always, local minima of cumulative throw at relay ramp locations (Peacock and Sanderson, 1994).

Solitario Canyon and Iron Ridge faults were plotted on a distance-throw graph (Fig. 5). The Solitario Canyon fault shows local displacement minima where Iron Ridge fault joins Solitario Canyon fault, and south of this intersection where NW trending faults are present. These minima can be explained by deformation within the relay ramp between Solitario Canyon and Iron Ridge faults and displacement transfer to Iron Ridge Fault. Individual faults normally have a bow or C-shaped throw profile, with maximum displacement near the center and zero displacement at the ends. The Iron Ridge fault does not show zero displacement at its northern end. The Iron Ridge fault, however, is no longer isolated. Instead it is physically linked (hard-linked) to Solitario Canyon faults.

Fault throws on the model were added to form a cumulative throw profile. The cumulative throw profile has non-zero displacement at the southern end because faults continue beyond the model range to the north and south. Local throw minima at approximately 4.8km, 5.9km, and 7km correspond to the following fault (or segment) intersections, respectively: the northern and middle sections of the Solitario Canyon fault, the Solitario Canyon and the Iron Ridge faults, and the middle and southern sections of the Solitario Canyon fault.

CONCLUSIONS

Other than Northern Windy Wash, which steepens from north to south, faults on western Yucca Mountain between UTM 544040 and 549000 do not show a correlation between dip angle and latitude. Large-scale fault-plane corrugations are evident on the Iron Ridge-Solitario Canyon fault system. Connecting faults are present between the Fatigue Wash and Northern Windy Wash faults. Connecting faults and curved tips trend NW (Ferrill *et al.*, 1998). The fault throw profile of Iron Ridge fault does not have a C-shape. It shows non-zero displacement at the northern end, where displacement is directly transferred to Solitario Canyon fault. Fault throw is high at cusps on Solitario Canyon and along connecting faults to the west, indicating an advanced state of fault interaction in which relay ramps have been breached.

Acknowledgements—I thank Ron Martin for sharing his technical computer expertise while training me for this project. I thank Darrell Sims for patiently teaching me concepts of fault scarp shapes and cumulative throw profiles, and for his good humor and encouragement. I thank David Ferrill, Stuart Birnbaum, and Eric Swanson for reviews which greatly improved the final paper, with special thanks to David Ferrill for sharing his extensive knowledge of structural geology and the geology of Yucca Mountain, for providing numerous articles about geologic studies of Yucca Mountain, and for his patient guidance throughout the project.

REFERENCES

Childs, C., Watterson, J. and Walsh, J.J. (1995) Fault overlap zones within developing normal fault systems. *Journal of the Geological Society, London* **152**, 535-549.

Dawers, N.H. and Anders, M.H. (1995) Displacement-length scaling and fault linkage. *Journal of Structural Geology* **17**, 607-614.

Dawers, N.H., Anders, M.H. and Scholz, C.H. (1993) Growth of normal faults: displacement-length scaling. *Geology* **21**, 1107-1110.

Day, W.C., Potter, C.J., Sweetkind, D.S., Dickerson, R.P., and San Juan, C.A., (1997) Bedrock Geologic Map of the Central Block Area, Yucca Mountain, Nye County, Nevada. U.S. Geological Survey Miscellaneous Investigations Investigation Series Map I-6201. Scale 1:6,000. U.S. Geological Survey, Denver, CO.

Day, W.C., Dickerson, R.P., Potter, C.J., Sweetkind, D.S., San Juan, C.A., Drake, R.M. II and Fridrich, C.J. (1998) Geologic Map of the Yucca Mountain Area, Nye County, Nevada, Draft. Scale 1:24,000. U.S. Geological Survey: Denver, CO.

Ferrill, D.A., Stirewalt, G.L., Henderson, D.B., Stamatakos, J.A. Morris, A.P., Wernicke, B.P., and Spivey, K.H. (1996) *Faulting in the Yucca Mountain Region: Critical Review and Analysis of Tectonic Data from the Central Basin and Range.* NUREG/CR-6401. U.S. Nuclear Regulatory Commission, Washington D.C..

Ferrill, D.A., Connor, C.B., Stamatakos, J.A., Mckague, H.L., Hill, B.E., Ofoegbu, G.I. and Terhune, R. (1997) *Modeling fault-dike interaction: implications for lateral diversion of dikes and alignment of volcanoes in the Yucca Mountain (Nevada)*

Region. CNWRA Intermediate Milestone 20-5708-471-760. Center for Nuclear Waste Regulatory Analyses: San Antonio, TX.

Ferrill, D.A., Stamatakos, J.A. and Sims, D., in press, Normal Fault Corrugation: Implications for Growth and Seismicity of Active Normal Faults. Submitted to *Journal of Structural Geology*.

Morris, A.P., Ferrill, D.A., and Henderson, D.B. (1996) Slip tendency analysis and fault reactivation. *Geology* **24**, 275-278.

Peacock, D.C. and Sanderson, D.J. (1994) Geometry and development of relay ramps in normal fault systems. *American Association of Petroleum Geology Bulletin* **78**, 147-165.

Sawyer, D.A., Fleck R.J., Lanphere, M.A., Warren, R.G., Broxton, D.E. and Hudson, M.R. (1994) Episodic caldera volcanism in the Miocene southwestern Nevada volcanic field: revised stratigraphic framework, $^{40}Ar/^{39}Ar$ geochronology, and implications for magmatism and extension. *Geological Society of America Bulletin* **106**, 1304-1318.

Scholz, C.H., Dawers, N.H., Yu, J.-Z. and Anders, M.H. (1993) Fault growth and fault scaling laws: preliminary results. *Journal of Geophysical Research* **98**, 21,951-21,961.

Scott, R.B. (1990) Tectonic setting of Yucca Mountain, southwest Nevada, in Wernicke, B.P. (ed.), Basin and Range Extensional Tectonics near the Latitude of Las Vegas, Nevada: Boulder, Colorado. *Geological Society of America Memoir* 176, p. 251-282.

Simonds, W.F.,Whitney, J.W., Fox, K., Ramelli, A., Yount, J.C., Carr, C.D., Menges, R., Dickerson, R. and Scott, R.B. (1995) Map of Fault Activity of the Yucca Mountain Area, Nye County, Nevada. U.S. Geological Survey Miscellaneous Investigations Series, Map

I-2520. Scale 1:24,000.

Stirewalt, G.L., Young, S.R. and Henderson, D.B. (1994) A Preliminary Three-Dimensional Model for Yucca Mountain, Nevada: Report to Accompany Model Transfer to the Nuclear Regulatory Commission. CNWRA 94-023. Center for Nuclear Waste Regulatory Analyses, San Antonio, TX.

Trudgill, B., and Cartwright, J. (1994) Relay-ramp forms and normal-fault linkages, Canyonlands National Park, Utah. *Geological Society of America Bulletin* **106**, 1143-1157.

Willemese, E.J. (1997) Segmented normal faults: correspondence between three-dimensional mechanical models and field data. *Journal of Geophysical Research* **102**, 675-692.

Willemese, E.J., Pollard, D.D., and Aydin, A. (1996) Three-dimensional analyses of slip distributions on normal fault arrays with consequences for fault scaling. *Journal of Structural Geology* **18**, 295-309.

FIGURE CAPTIONS

Table 1. Fault orientation data for Northern Windy Wash, Fatigue Wash, Boomerang Point, Solitario Canyon, Iron Ridge faults, complied from maps by Simonds *et al.* (1995) and Day *et al.* (1998). Coordinates are in UTM zone 11, NAD83.

Fig 1. Fault dip versus latitude for (a) Northern Windy Wash, (b) Fatigue Wash, (c) Boomerang Point, (d) Solitario Canyon, and (e) Iron Ridge faults. Orientation data for the Northern Windy Wash fault show an increase in fault dip to the south, whereas orientation data for Fatigue Wash, Boomerang Point, Solitario Canyon, and Iron Ridge faults show no pronounced along-strike trend.

Fig 2. Three-dimensional model of major faults of western Yucca Mountain. The five major N-S faults are, from west to east, Northern Windy Wash, Fatigue Wash, Boomerang Point, Solitario Canyon, and Iron Ridge faults. Only the west-dipping portion of Solitario Canyon Fault is included. Fault dips are the average dips shown in Table 1. Also shown with 80 degree dips are a fault between Northern Windy Wash and Fatigue Wash faults, and a fault within the relay ramp between Iron Ridge and Solitario Canyon faults. Coordinates labeled on the model are in meters. Long horizontal dimension of model = 14900m, short horizontal dimension of model = 4954m, vertical dimension of model = 1340m.

Fig. 3. (a) White points indicate data points used to build the 3D model of the bottom of Cr in the Miocene Tiva Canyon Tuff. At each point, the bottom of Cr, a crystal-rich member of the Tiva

Canyon Tuff is exposed at the Earth's surface. (b) Three-dimensional model of major faults shown in Figure 2 and the horizon defined by the bottom of Cr. Block dimensions are the same as in Figure 2.

Figure 4. Evolution of fault growth and relay ramp development. (a) Breakthrough of an en echelon array by curved lateral propagation causes large scale corrugations. Relict fault tips are depicted on the hangingwall. Only one relict fault tip occurs in the area of fault overlap. (b) Breakthrough by connecting fault formation eventually leads to individual segments with large centers and small relict tips. Connecting faults are often nearly as large as segments. Here, two relict fault tips occur per area of fault overlap. Fault tips are shown in both the hangingwall and the footwall. From Ferrill *et al.*, 1998.

Figure 5. Yucca Mountain distance versus throw profiles. Solitario Canyon fault is the heavy solid line, and Iron Ridge fault is the light solid line. The cumulative throw profile (dashed line) is the sum of throws of Solitario Canyon and Iron Ridge faults. Local throw minima at approximately 4.8km, 5.9km, and 7km correspond to the following fault (or segment) intersections, respectively: the northern and middle sections of the Solitario Canyon fault, the Solitario Canyon and Iron Ridge faults, and the middle and southern sections of the Solitario Canyon fault.

Data Source	UTM Coordinates		Strike	Dip
Northern Windy Wash				
Day et. al	545139.53	4083696	309	46
Day et. al	545107.71	4082908.7	1	55
Day et. al	545121.31	4082718.2	353	55
Day et. al	545033.64	4082103.6	5	64
Day et. al	544948.63	4081652	25	65
Day et. al	544936.41	4081580.6	329	78
Day et. al	544927.8	4081114.6	320	80
Day et. al	545034.51	4080953.5	350	80
			Dip average	65
Fatigue Wash Fault				
Day et. al	545020.01	4078247.3	1	72
Day et. al	544841.89	4077672	359	70
Day et. al	544756.53	4077365.7	359	80
			Dip average	74
Boomerang Point Fault				
Day et. al	545942.68	4078040.6	218	85
			Dip average	85
Solitario Canyon				
Day et. al	547411.83	4080386	13	85
Day et. al	547452.23	4079346.3	8	75
Day et. al	547407.46	4079222.3	15	70
Day et. al	547299.3	4078357.7	358	80
Day et. al	547349.08	4077985.8	23	70
Day et. al	547272.21	4077905	1	75
Day et. al	547267.56	4077815.5	356	80
Day et. al	546920.59	4076914.8	7	80
Day et. al	546888.44	4076841.2	6	65
Day et. al	546876.94	4076813.7	2	76
Day et. al	546843.15	4076738.2	8	80
Day et. al	546887.93	4076340.4	331	55
Day et. al	547018.29	4075887.2	2	66
Day et. al	547021.93	4075769.5	15	56
Day et. al	547017.62	4076117.3	301	52
Day et. al	547029.88	4076008.5	8	48
Day et. al	547055.79	4075352	341	73
Day et. al	547077.98	4075301.8	339	65

Data Source	UTM Coordinates		Strike	Dip
Solitario Canyon (continued)				
Day et. al	546614.02	4073868.3	355	69
Day et. al	546612.11	4073834.5	354	66
Day et. al	546585.65	4073254.2	354	48
Day et. al	546580.22	4073026.3	360	62
Day et. al	546544.58	4072851.8	4	75
Day et. al	546409.5	4072160.6	4	55
Simonds et. al	546182.82	4071367.5	360	81
Simonds et. al	546249.72	4071594.8	63	80
Simonds et. al	546276.33	4071705.8	352	52
Simonds et. al	546319.67	4071760.6	1	85
Simonds et. al	546318.59	4071761.5	5	85
Simonds et. al	546349.59	4071848.3	5	60
Simonds et. al	546360.81	4071915.3	4	60
Simonds et. al	546367.31	4072005.3	357	66
Simonds et. al	546222.65	4071939.2	8	76
Simonds et. al	546480.46	4072697.4	27	68
Simonds et. al	546497.34	4072793.4	3	72
Simonds et. al	546528.99	4072939	21	70
Simonds et. al	546554.31	4073019.2	24	70
Simonds et. al	546571.18	4073121.5	358	58
Simonds et. al	546582.79	4073461.2	347	80
Simonds et. al	546602.4	4073646.1	333	56
Simonds et. al	546611	4073791.8	360	69
Simonds et. al	546610.09	4073842.5	29	72
Simonds et. al	546597.88	4073923	339	61
Simonds et. al	546839.55	4074441.6	7	60
Simonds et. al	547002.44	4074685.8	34	68
Simonds et. al	547050.38	4074781.3	23	60
Simonds et. al	547078.1	4074831.9	27	60
Simonds et. al	547098.57	4074926.2	6	80
Simonds et. al	547067.42	4075318.9	348	70
Simonds et. al	547067.39	4075318.9	348	65
Simonds et. al	547001.74	4075775.2	4	57
Simonds et. al	547011.25	4075978.1	9	54
Simonds et. al	547016.73	4076011.8	7	53
Simonds et. al	546951.68	4076073.6	325	75
Simonds et. al	547021.52	4076130.5	344	48
Simonds et. al	547004.73	4076175.9	330	52
Simonds et. al	546855.24	4076444.5	352	55
Simonds et. al	546839.41	4076541.5	2	61

Table 1

Data Source	UTM Coordinates		Strike	Dip		Data Source	UTM Coordinates		Strike	Dip
Solitario Canyon (continued)						Iron Ridge				
Simonds et. al	546855.41	4076663.5	81	70		Day et. al	547674.73	4073145.3	359	65
Simonds et. al	546834.25	4076798.5	34	80		Simonds et. al	547779.61	4071683	351	58
Simonds et. al	546871.38	4076882.1	21	85		Simonds et. al	547808.25	4071495.6	15	70
Simonds et. al	547125.15	4077241.3	28	75		Simonds et. al	547781.36	4071299.7	23	72
Simonds et. al	547125.69	4077241.2	28	75		Simonds et. al	547792.25	4070958.2	16	84
Simonds et. al	547142.48	4077468.8	338	80		Simonds et. al	547800.9	4070867.6	311	55
Simonds et. al	547180.63	4077616.8	359	70		Simonds et. al	547796.4	4070355.9	3	80
Simonds et. al	547228.75	4077809.8	9	80		Simonds et. al	547777.75	4070210.8	357	70
Simonds et. al	547236.57	4077832.4	31	75		Simonds et. al	547770.2	4070096.7	20	75
Simonds et. al	547247.4	4077878.9	353	75		Simonds et. al	547728.7	4069809.7	7	75
Simonds et. al	547287.95	4078353.5	13	80		Simonds et. al	547709	4069658.5	10	60
Simonds et. al	547402.71	4080381.7	9	85		Simonds et. al	547655.79	4069432.5	4	65
Simonds et. al	547436	4080570	13	60		Simonds et. al	547606.16	4069191.8	4	73
Simonds et. al	547445.06	4080629.3	360	60		Simonds et. al	547543.8	4068921.4	18	80
Simonds et. al	547468.01	4080749.5	3	65		Simonds et. al	547497.3	4068773.6	35	80
Simonds et. al	547559.3	4081445.3	28	86		Simonds et. al	547510.31	4068568.5	4	65
Simonds et. al	547680.1	4082965.5	358	80		Simonds et. al	547536.93	4068466.6	339	75
Simonds et. al	547676.07	4083182.5	356	85		Simonds et. al	547535.9	4068291.6	344	75
			Dip average	76		Simonds et. al	547702.64	4067953.1	119	70
						Simonds et. al	547733.98	4067975.5	341	70
						Simonds et. al	547796.06	4067851.2	136	60
						Simonds et. al	547893.7	4067730.1	338	60
						Simonds et. al	548011.69	4067283.1	315	65
									Dip average	70

Table 1 (continued)

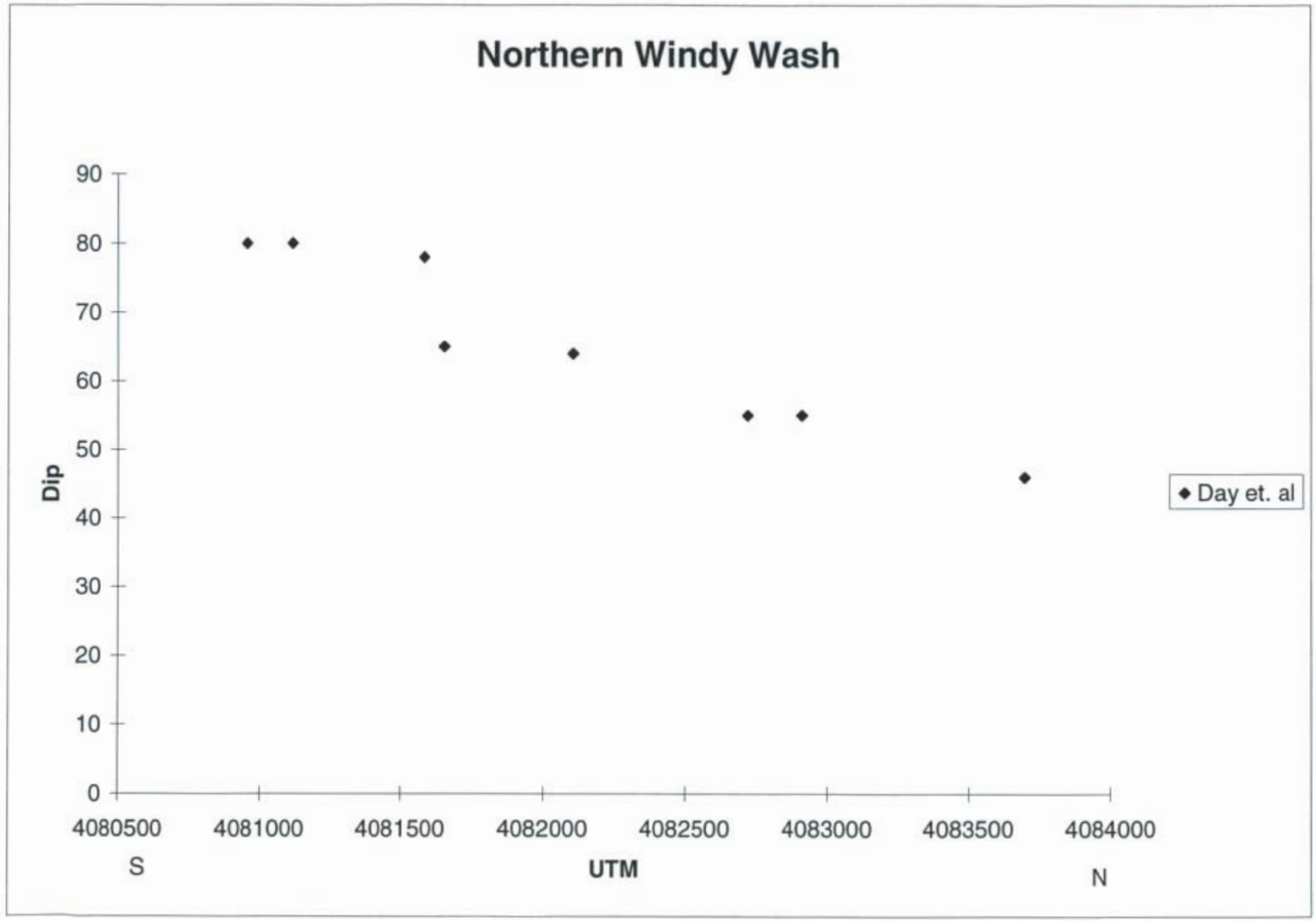

Northern Windy Wash
90
80
70
60
50
40
30
20
10
0
Dip
4080500
4081000
4081500
4082000
4082500
4083000
4083500
4084000
S
UTM
N
Day et. al

Figure 1a.

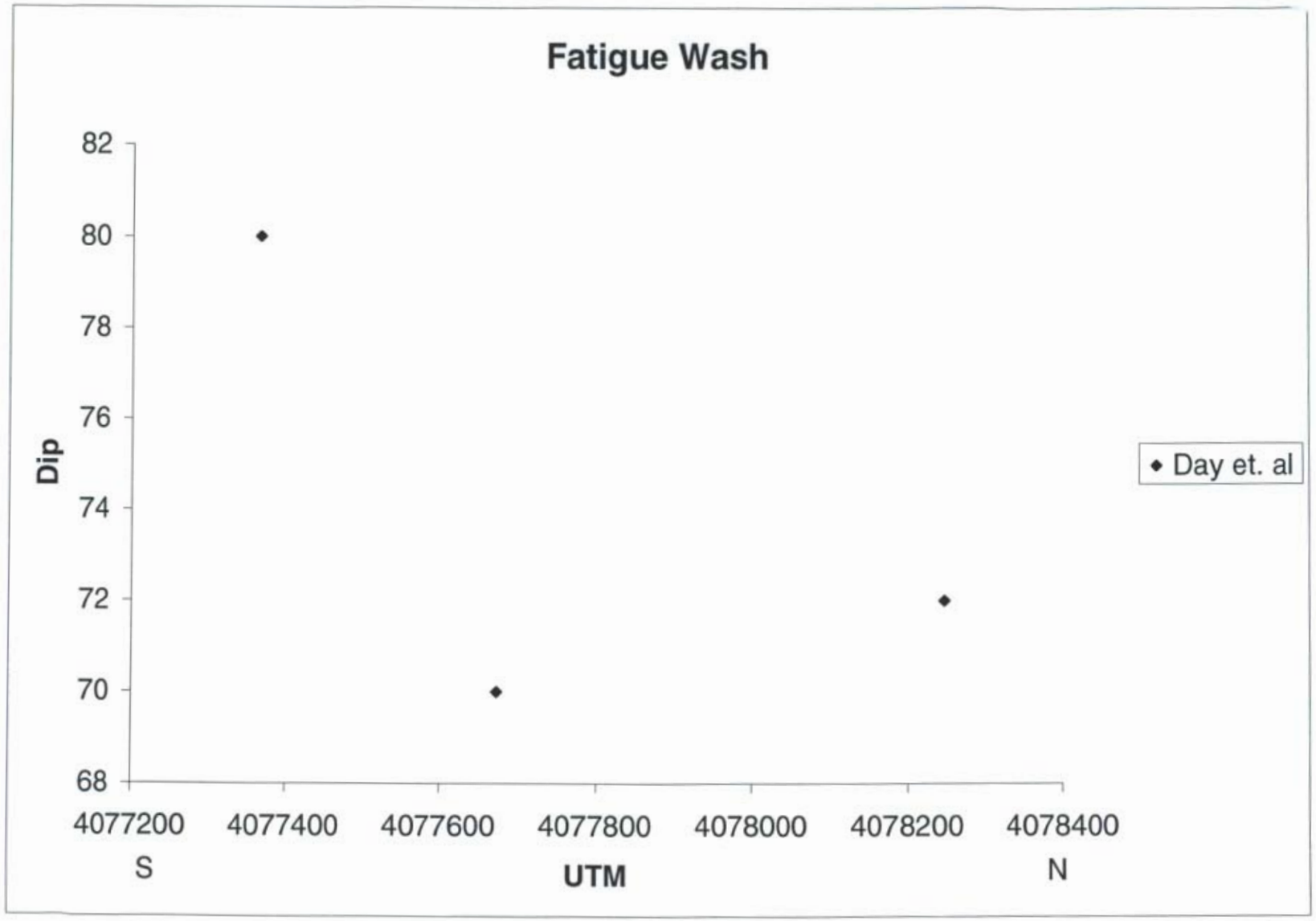

Fatigue Wash
82
80
78
76
74
72
70
68
Dip
4077200
4077400
4077600
4077800
4078000
4078200
4078400
S
UTM
N
Day et. al

Figure 1b.

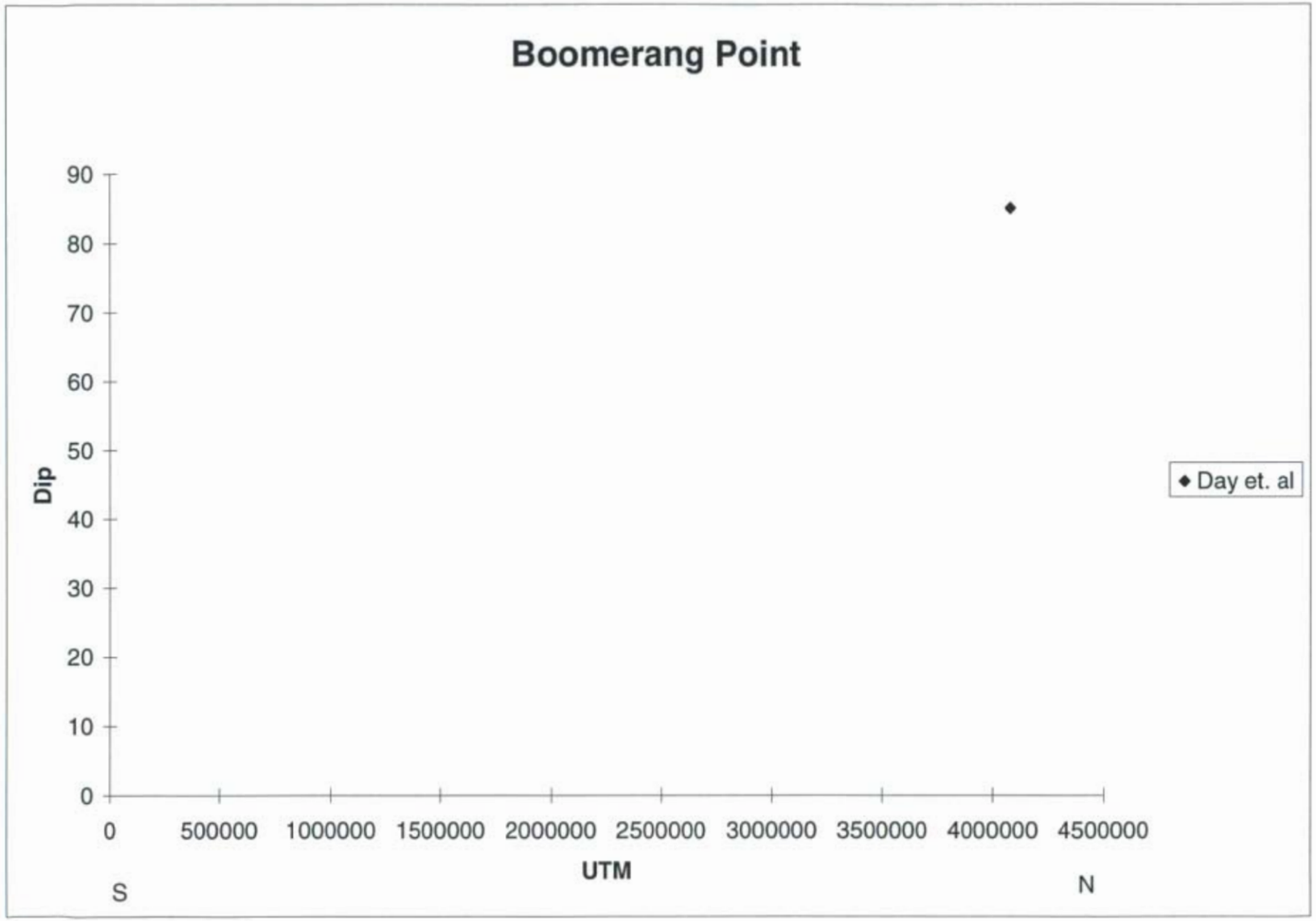

Boomerang Point
90
80
70
60
50
40
30
20
10
0
Dip
0
500000
1000000
1500000
2000000
2500000
3000000
3500000
4000000
4500000
UTM
S
N
◆ Day et. al

Figure 1c.

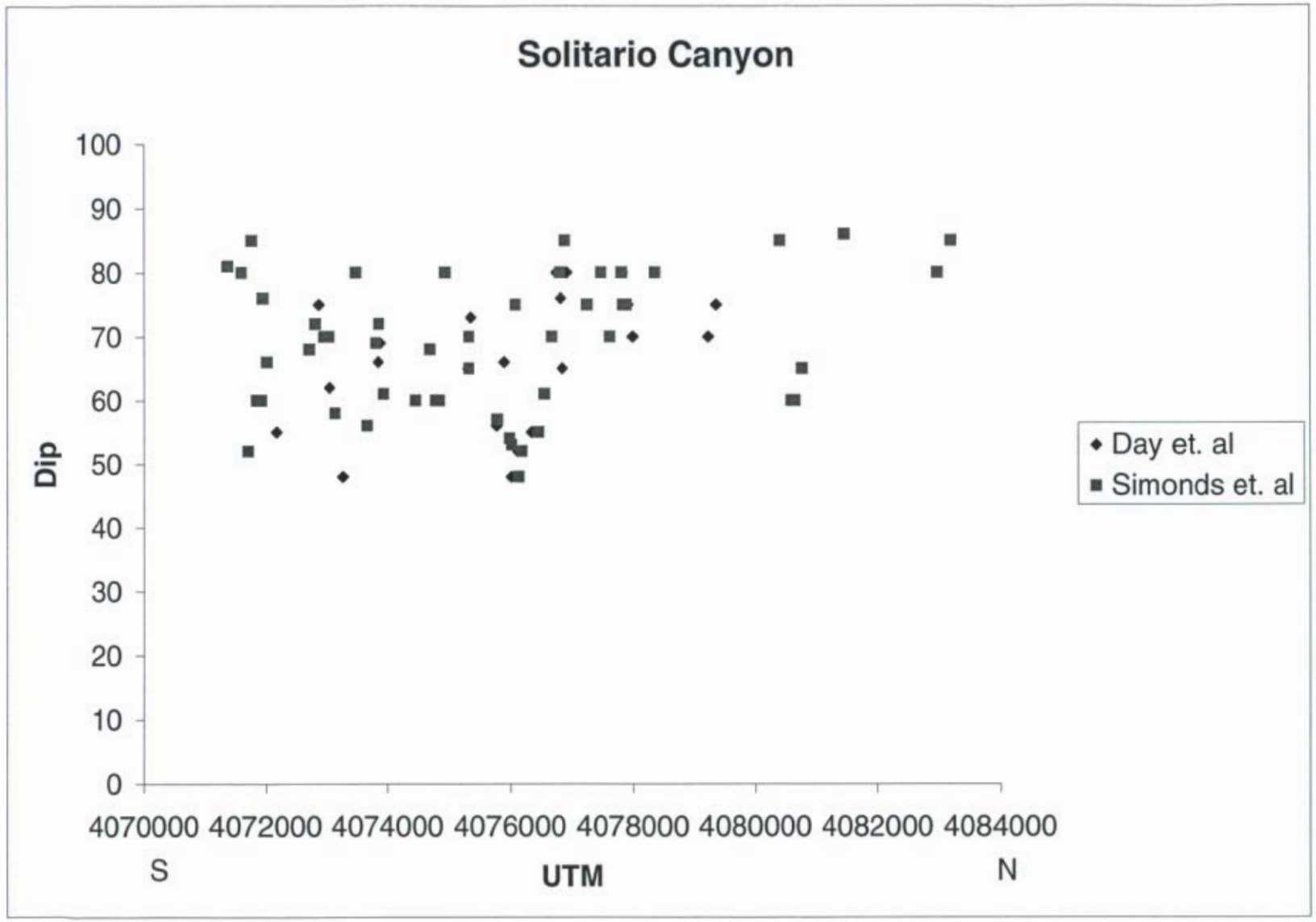

Solitario Canyon
100
90
80
70
60
50
40
30
20
10
0
Dip
4070000 4072000 4074000 4076000 4078000 4080000 4082000 4084000
S
UTM
N
Day et. al
Simonds et. al

Figure 1d.

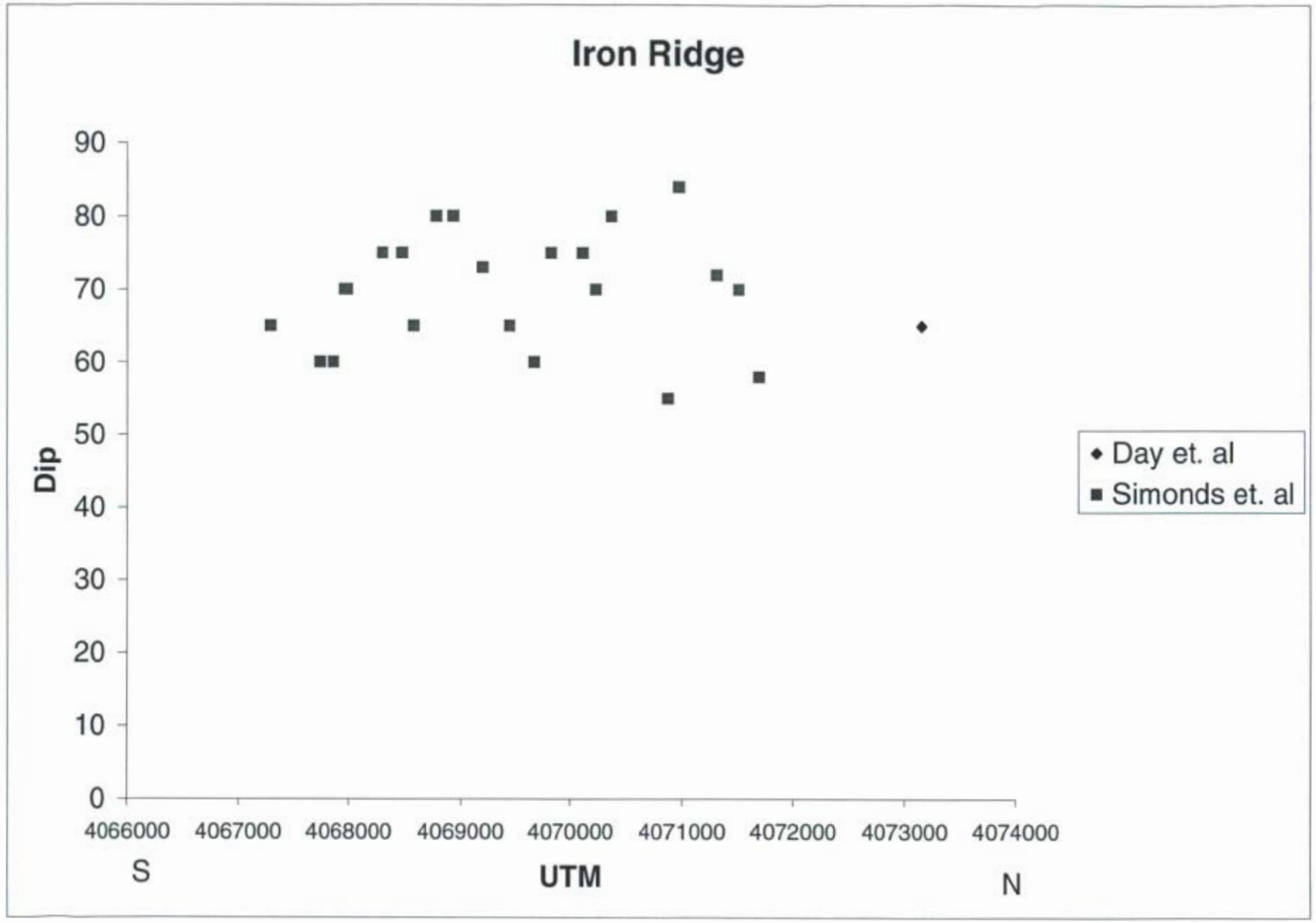

Iron Ridge
90
80
70
60
50
40
30
20
10
0
Dip
4066000
4067000
4068000
4069000
4070000
4071000
4072000
4073000
4074000
S
UTM
N
Day et. al
Simonds et. al

Figure 1e.

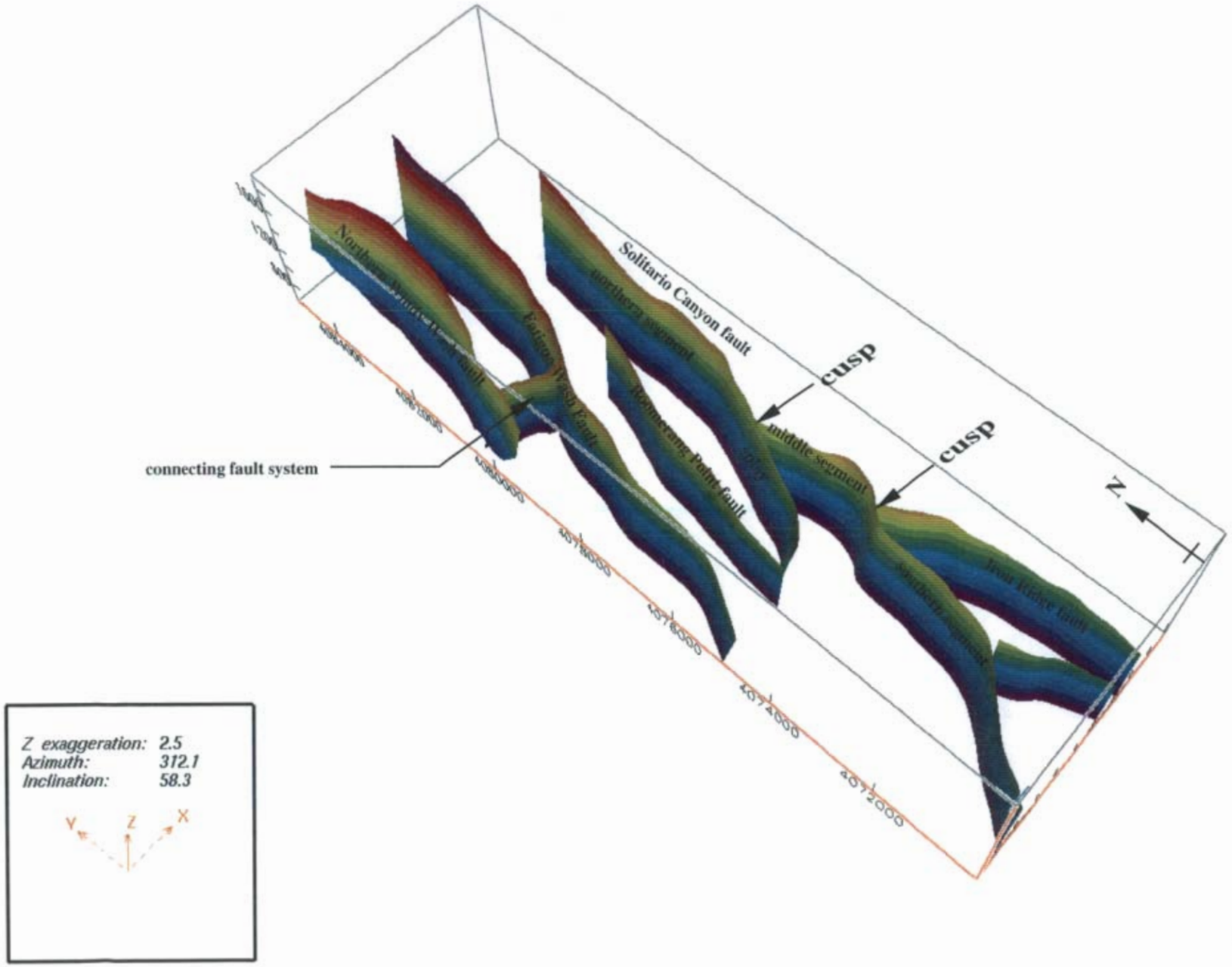

Solitario Canyon fault
northern segment
cusp
cusp
middle segment
Z
connecting fault system
Z exaggeration: 2.5
Azimuth: 312.1
Inclination: 58.3
Y
Z
X

Figure 2.

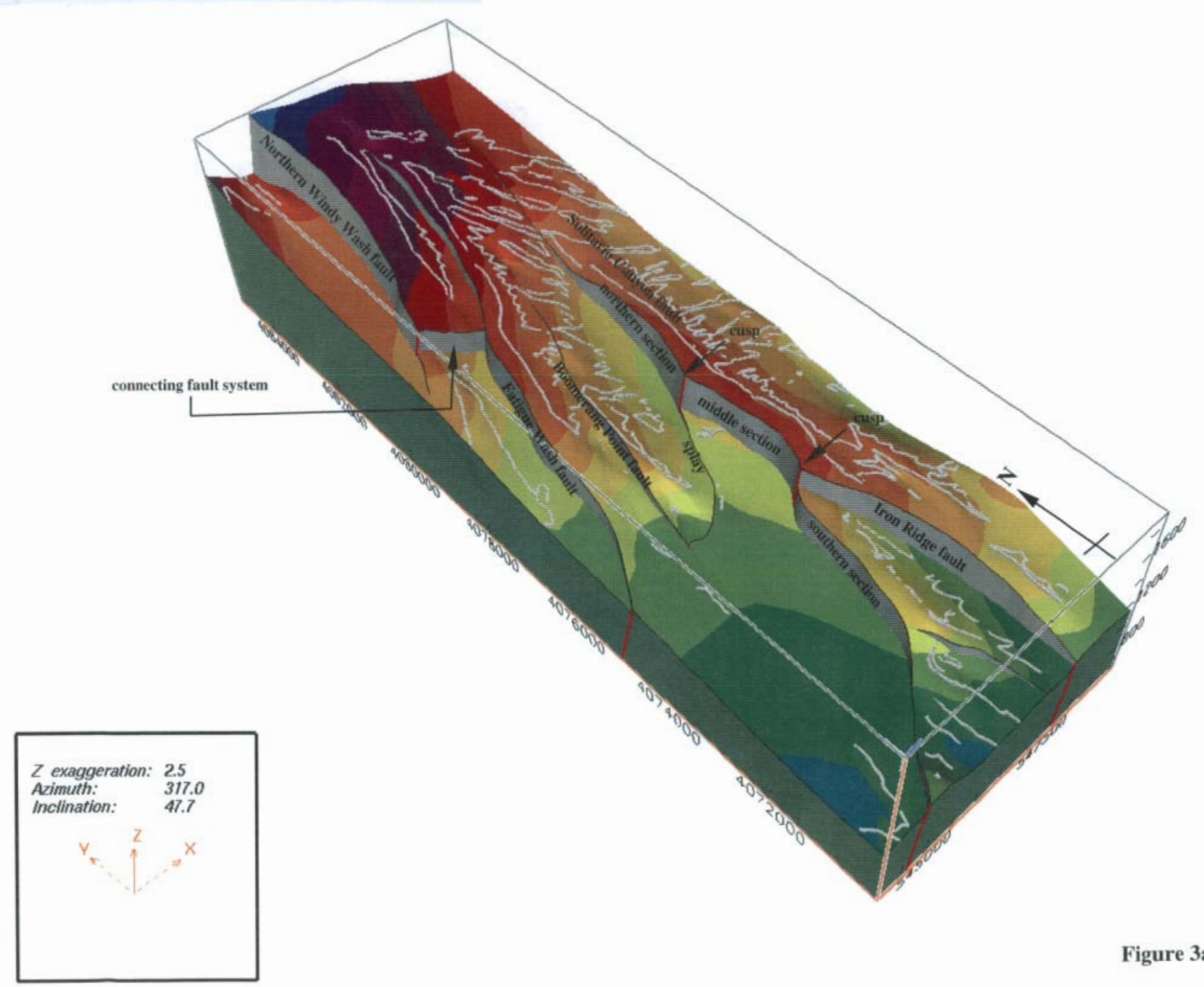
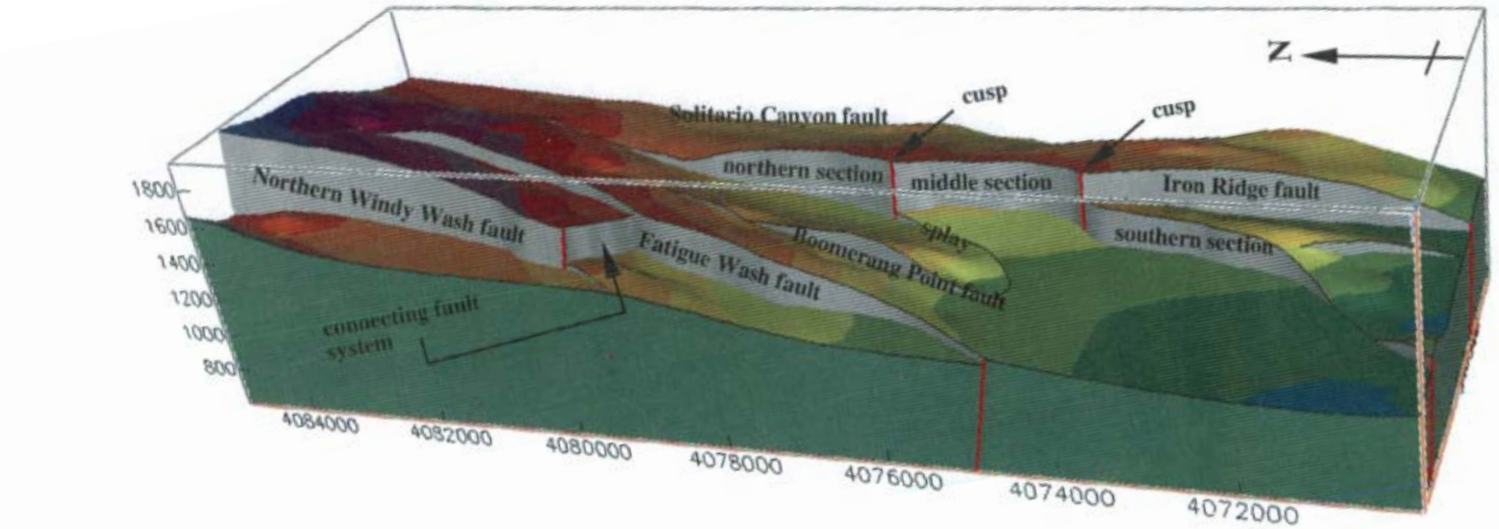

Northern Windy Wash fault
Solitario Canyon fault
northern section
cusp
connecting fault system
Ranger Peak fault
Fatigue Wash fault
splay
middle section
cusp
Iron Ridge fault
southern section
Z
4078000
4076000
4074000
4072000
Z exaggeration: 2.5
Azimuth: 317.0
Inclination: 47.7
Z
Y
X

Figure 3a.


Z
Solitario Canyon fault
cusp
cusp
northern section
middle section
Iron Ridge fault
Northern Windy Wash fault
splay
southern section
Fatigue Wash fault
Boomerang Point fault
connecting fault system
1800
1600
1400
1200
1000
800
4084000
4082000
4080000
4078000
4076000
4074000
4072000

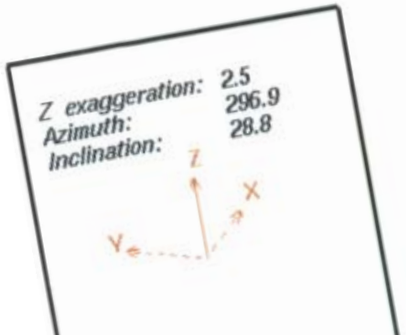

Z exaggeration: 2.5
Azimuth: 296.9
Inclination: 28.8
Z
X
Y

Figure 3b.

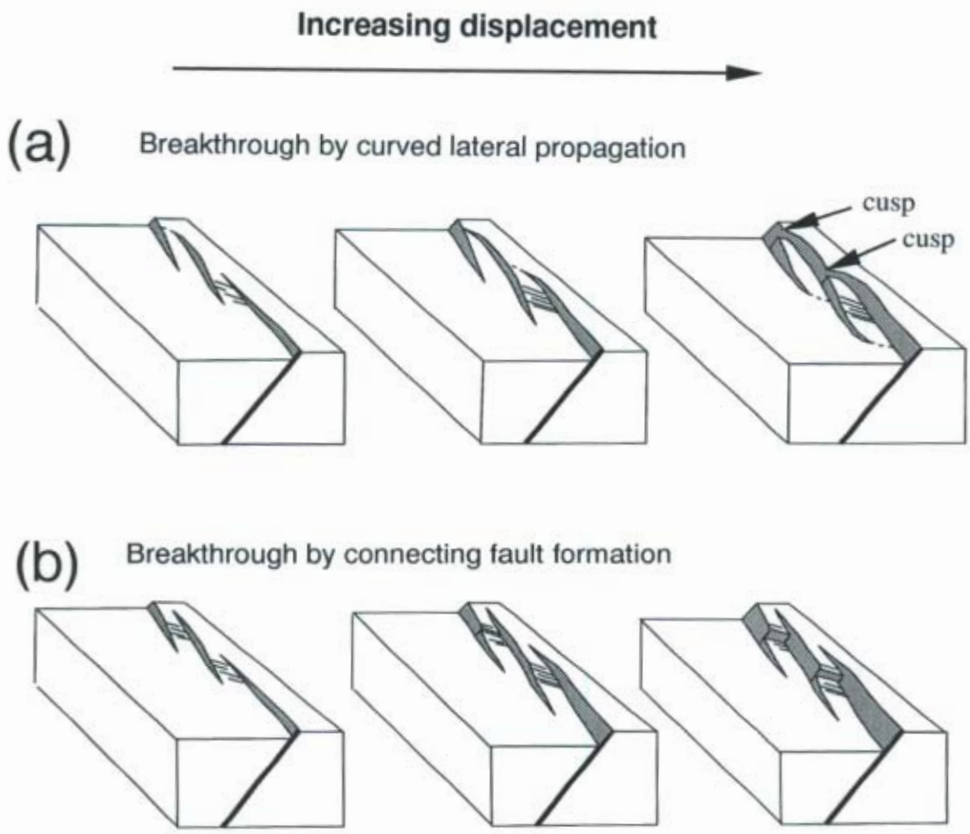

Increasing displacement
(a)
Breakthrough by curved lateral propagation
cusp
cusp
(b)
Breakthrough by connecting fault formation

Figure 4.

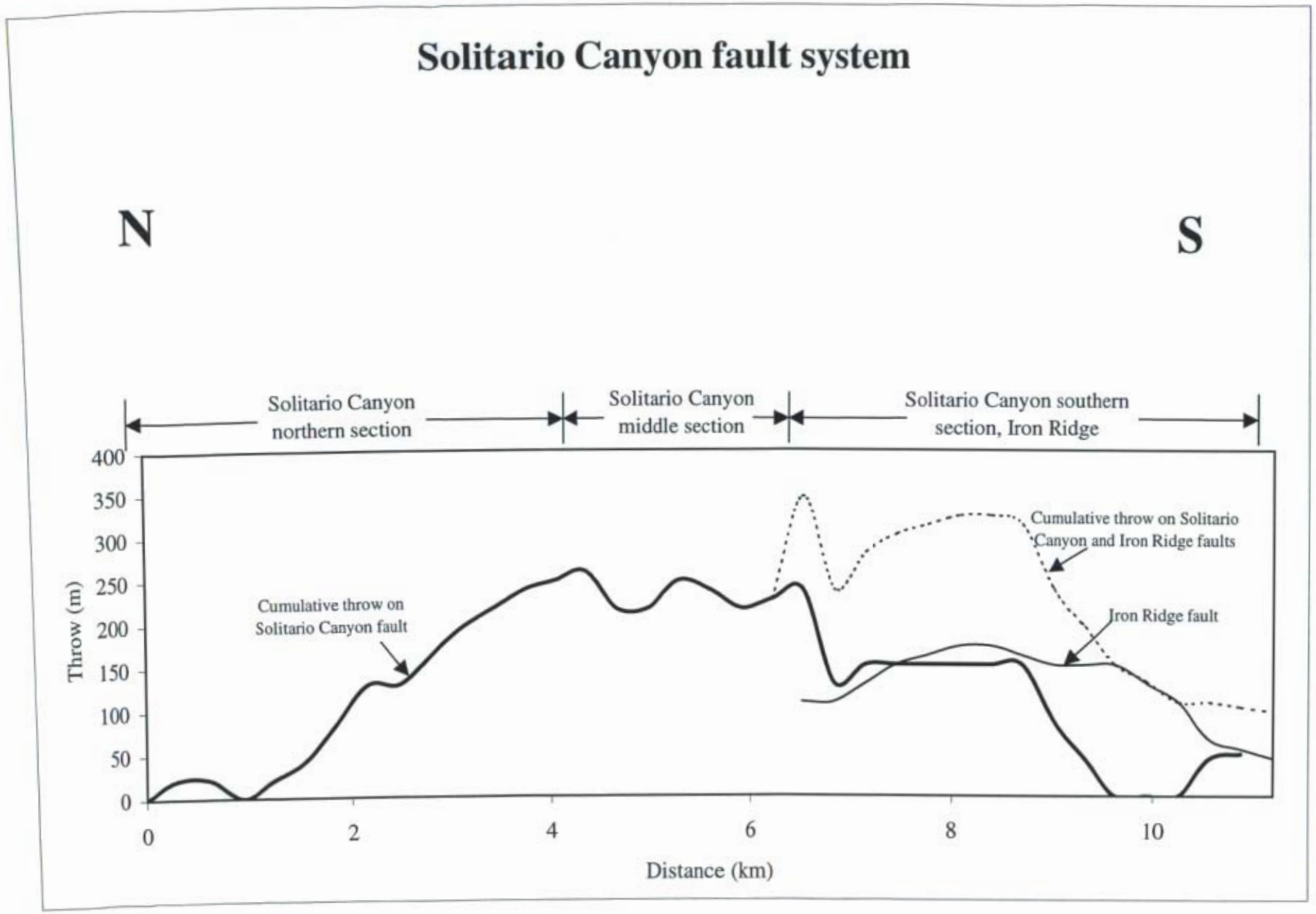

Solitario Canyon fault system
N
S
Solitario Canyon northern section
Solitario Canyon middle section
Solitario Canyon southern section, Iron Ridge
Cumulative throw on Solitario Canyon and Iron Ridge faults
Cumulative throw on Solitario Canyon fault
Iron Ridge fault
Throw (m)
400
350
300
250
200
150
100
50
0
0
2
4
6
8
10
Distance (km)

Figure 5.